Chapter 2

Interaction of Small Molecules within Metal Organic Frameworks Studied by *In Situ* Vibrational Spectroscopy

Kui Tan and Yves Jean Chabal

Additional information is available at the end of the chapter

http://dx.doi.org/10.5772/64906

Abstract

Molecular-level characterization of interaction between small gases and metal organic frameworks (MOFs) is crucial to elucidate the adsorption mechanism and establish the relationship between the structure and chemical features of MOFs with observed adsorptive properties, which ultimately guide the new structure design and synthesis for enhanced functional performance. Among different techniques, vibrational spectroscopy (infrared and Raman), which provides fingerprint of chemical bonds by their vibrational spectra, is one of the most powerful tools to study adsorbate-adsorbent interaction and give rich detailed information for molecular behaviors inside MOFs pores. This chapter reviews a number of exemplary works utilizing vibrational spectroscopy to study the interaction of small molecules with metal organic frameworks.

Keywords: interaction, small molecules, metal organic frameworks (MOFs), infrared (IR), Raman spectroscopy, vdW-DF calculation

1. Introduction

In the past decade, metal organic frameworks (MOFs) have become one of the fastest growing new fields in chemistry. Tremendous advances has been made in synthesis for new structures (>20,000 reported), structure determination or postmodification, and exploration of potential application in different fields such as gas storage and separation (H_2, CO_2, N_2, and CO_2), drug delivery, sensing, luminescence, and catalysis based on adsorption. The mechanistic understanding of the interaction of the molecules with MOFs is critical for the rational design of new MOFs with desired properties and accurate assessment of functional perform-

ance in practical applications. Traditional characterization methods for MOFs materials have relied mainly on physical measurements, such as X-ray diffraction, thermogravimetric, gas adsorption isotherm, and breakthrough analysis. These techniques are powerful in deriving some critical parameters, such as crystal structures, chemical composition, thermal stability, adsorptive uptake, enthalpy, and selectivity, for assessing adsorption properties; however, mechanistic information about the local bonding sites, adsorption geometry, and guest-host, guest-guest cooperative, or competitive interaction is particularly difficult to derive. Experimental methods currently employed by the community to analyze how the molecules interact with a framework include infrared and Raman spectroscopy, X-ray (neutron) diffraction, and inelastic neutron scattering. While all these techniques have been shown to be useful to identify the binding sites of the MOFs toward the small molecules, vibration spectroscopy, i.e., infrared and Raman spectroscopy is particularly sensitive to probe the local interaction between guest molecules and the surface of metal organic frameworks. These two spectroscopic techniques provide complementary information about the nature of interaction, bonding configurations, intermolecular attraction, or repulsion through their vibrational spectra. Furthermore, they require lower capital cost and have greater accessibility of the instrumentation, which is easily modified for *in situ* measurements in a wide range of temperatures and pressures.

In this chapter, the recent progress of infrared and Raman spectroscopy studies on the underlying interactions that govern adsorption behaviors of small molecules, i.e., H_2, CO_2, H_2O, O_2, CO, NO, H_2S, SO_2, in different MOFs materials is discussed and summarized. In most cases for nonreactive molecules, such as H_2 and CO_2, van der Waals forces dominate the interaction between the guest molecules and the building units of the MOFs. In some cases, chemical reaction involving electron transfer occurs upon adsorption of reactive molecules, e.g., H_2O, leading to a significant modification of MOFs crystalline structure. Combined with calculation, especially the recent successful effort to include van der Waals forces, self-consistently in DFT(Density functional theory) in the form of a van der Waals density functional, molecular weak physical interactions within MOFs materials are accurately described and experimental data can be well interpreted and rationalized.

2. Interaction of small molecules with MOFs

2.1. Energy carrier H_2

H_2 molecule is IR inactive as other homonuclear diatomic molecules due to their lack of dipole moment; however, once the molecule interacts with the MOF, it undergoes a perturbation that polarizes the originally symmetric molecule and makes it weakly IR active. This perturbation is usually accompanied by red shift of the H—H stretching modes, located at 4161 and 4155 cm^{-1} for para and ortho H_2, respectively. Nijem's measurement on different type of prototypical MOFs suggest that magnitudes of the H_2 stretching frequency shifts, intensities, and line widths contains important information about the nature of the H_2 interaction in the pores and depend on the structure and chemical nature of the MOF hosts [1].

http://dx.doi.org/10.5772/64906

By examining several prototypes of metal organic framework materials such as M(bdc)$(ted)_{0.5}$ (bdc = 1, 4-benzenedicarboxylate; ted = triethylenediamine), M(bodc)$(ted)_{0.5}$ (M = Ni, Co; bodc = bicyclo[2. 2. 2]octane-1, 4-dicarboxylate), $M_3(HCOO)_6$ (M = Ni, Mn, Co, HCOO = formate), and $Zn_2(bpdc)_2(bpee)$, where bpdc = 4,4′-biphenyl dicarboxylate and bpee = 1,2-bis(4-pyridyl)ethylene [1], it is concluded (see **Table 1**) that IR shifts are dominated by the environment (organic ligand, metal center, and structure) rather than the strength of the interaction. For instance, the organic ligands with π = electrons such as benzene rings cause the frequency of H_2 shift more than the ligand without π = electrons, e.g., H_2 bands are more shifted (~−3 cm^{-1}) for Ni(bdc)$(ted)_{0.5}$ than Ni(bodc)$(ted)_{0.5}$ even though Ni(bodc)$(ted)_{0.5}$ has a higher binding energy. The same observation was also found by comparing the IR shift (−38 cm^{-1}) of hydrogen molecules in Zn(bdc)$(ted)_{0.5}$ with that (−30 cm^{-1}) in MOF-74 (also called $M_2(dobdc)$, M = metal ions; $dobdc^{4-}$= 2,5-dioxidobenzene-1,4-dicarboxylate), a structure containing unsaturated metal center Zn^{2+} with a higher binding energy (10 kJ/mol).

MOF	Ligand type	Δν(H—H) (cm^{-1})	Fwhm (cm^{-1})	Pore structure/size (Å)	Binding energy (kJ/mol)
Zn(bdc)$(ted)_{0.5}$	Aromatic, aliphatic	−38	20	3D/~7.8	5–5.3
Ni(bdc)$(ted)_{0.5}$	Aromatic, aliphatic	−37	20	3D/7.8	NA
Cu(bdc)$(ted)_{0.5}$	Aromatic, aliphatic	−38	20	NA	4.9–6.1
Ni(bodc)$(ted)_{0.5}$	Aliphatic	−34	32	1D/~7–7.3	5.7–6.5
$Ni_3(COOH)_6$	Short aliphatic	−30	13	1D/~5–6	8.3–6.5
$Mn_3(COOH)_6$	Short aliphatic	−28	13	1D/~5–6	NA
$Co_3(COOH)_6$	Short aliphatic	−28	12	NA	NA
$Zn_2(bpdc)_2(bpee)$	Sromatic	−38	16	1D/~5×7	9.5_{viral}, 8.8_{poly}

Reprinted with permission from [1]. Copyright (2010) American Chemical Society.

Table 1. Comparison between the different properties of the different MOFs.

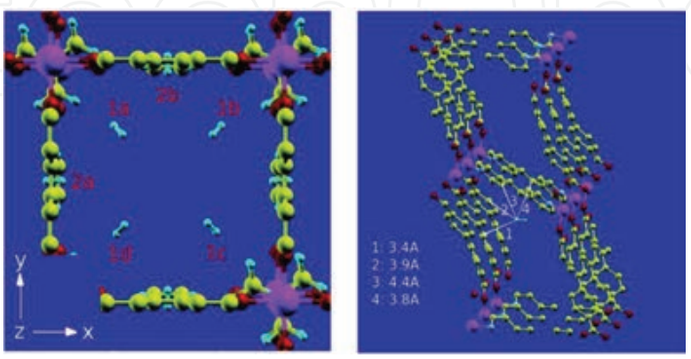

Figure 1. Hydrogen adsorption sites in Zn(bdc)$(ted)_{0.5}$ (left) and $Zn_2(bpdc)_2(bpee)$ (right). The interaction lines between one of the H atoms and carbon atoms in four different ligands are illustrated. Reprinted with permission from [1]. Copyright (2010) American Chemical Society.

Integrated intensity of the H_2 stretching modes is a sensitive measure of the number and symmetry of the sites and local interaction between H_2 and organic ligand. Asymmetric site with multiple interaction points produced larger induced dipole moment and the corresponding IR cross-section is higher [1]. The symmetric sites lead to reduced dynamic dipole moment and lower the IR band intensity. **Figure 1** compares the adsorption site of H_2 in M(bdc)$(ted)_{0.5}$ and $Zn_2(bpdc)_2(bpee)$: H_2 interacts with several benzene rings in $Zn_2(bpdc)_2(bpee)$ and the adsorption site is very asymmetric. Furthermore, the delocalized electrons in the double benzene rings in $Zn_2(bpdc)_2(bpee)$ is more easily polarized by adsorbed H_2 than that in the single benzene ring in Zn(bdc)$(ted)_{0.5}$. All these factors cause IR intensity of H_2 adsorbed in $Zn_2(bpdc)_2(bpee)$ almost a magnitude higher than that of H_2 adsorbed in M(bdc)$(ted)_{0.5}$.

It is worth to note that IR is not only sensitive to host-gust interaction but also capable to detect molecular interactions within confined nanopores. In MOF-74 with unsaturated metal center, a small shift (−30 cm^{-1} with respect to the unperturbed molecules) is observed in the low loading regime when H_2 is dominantly adsorbed on the metal site [2]. Additional ~−32 cm^{-1} IR shift and a large variation in dipole moment are observed once the neighboring oxygen site was occupied with H_2 molecule to form a "pair" with H_2 molecules on the metal site. Since large variation of dynamic dipole moment take place as a function of loading, due to the interaction among the adsorbed molecules and therefore the integrated areas of IR bands do not always correlate with the amount of molecules adsorbed. Cautions must be taken when using variable temperature IR to measure the absorbance of molecular hydrogen bands and estimate the adsorption energy [3].

2.2. Greenhouse emission CO_2

CO_2 is a linear molecule and has large quadrupole moment and high polarizability. The symmetric stretching mode (ν_1, 1342 cm^{-1}) is Raman active but not IR active, whereas the antisymmetric modes (β, 667 cm^{-1} and ν_3, 2349 cm^{-1}) are IR active. By interaction with adsorbent surface, the frequency position is perturbed and the adsorption band is affected.

Upon adsorption of CO_2 onto the active binding site of open metal ions within M-MOF-74 systems (M = Mg^{2+}, Zn^{2+}, Ni^{2+}, Co^{2+}, Mn^{2+}), the induced frequency shift of antisymmetric mode ν_3 is highly dependent on the nature of metal ions: it undergoes a blue shift in Mg^{2+} MOF while red shifts in Zn^{2+} MOF and other transitional metal analogs as shown in **Figure 2** [4, 5]. *Ab initio* calculations were performed in Mg^{2+} and Zn^{2+} MOFs utilizing vdW-DF, finding three factors contributing to this shift, i.e., namely, (i) the change in the molecule length, CO_2 molecules in Zn-MOF-74 experiences a larger elongation (0.0009 Å) than in Mg-MOF-74 (0.0009 Å), (ii) the asymmetric distortion of the CO_2 molecule, the asymmetric distortion in Mg-MOF-74 is stronger than that in Zn-MOF-74, which is consistent with a larger blue shift effect in the CO_2 ν_3 frequency, and (iii) the direct influence of the metal center. Specifically, the presence of the d orbitals in Zn^{2+} prevents the charge density transfer within the adsorbed CO_2 molecules, leading to small charge transfer compared to Mg^{2+} case [4].

Splitting of bending mode $\beta(CO_2)$ due to the removal of degeneracy of the in-plane and out-of-plane bending is commonly observed in the case of electron-donor-acceptor (EDA) com-

http://dx.doi.org/10.5772/64906

plexes of CO_2 with basic functional groups in polymer such as —NH_2, —OH via carbon of CO_2 as an electron acceptor [7]. The earliest spectroscopic evidences for the formation of an electron-donor-acceptor complex between CO_2 and functional groups of MOFs was reported in a MOF of type MIL-53 (MIL stands for Materials Institute Lavoisier) and amino-based MOF Zn_4O $(NH_2\text{-BDC})_3$ (IR-MOF-3) and (NH_2-MIL-53(Al) [6, 8]. Two bands at 669 and 653 cm^{-1} in **Figure 3**, corresponding bending mode of CO_2 was observed, indicating a lowering of symmetry upon adsorption. Moreover, ν(OH) and δ(OH) modes are red shifted by −19 and −30 cm^{-1}, respectively, suggesting that oxygen atoms of hydroxyl group act as the electron donor.

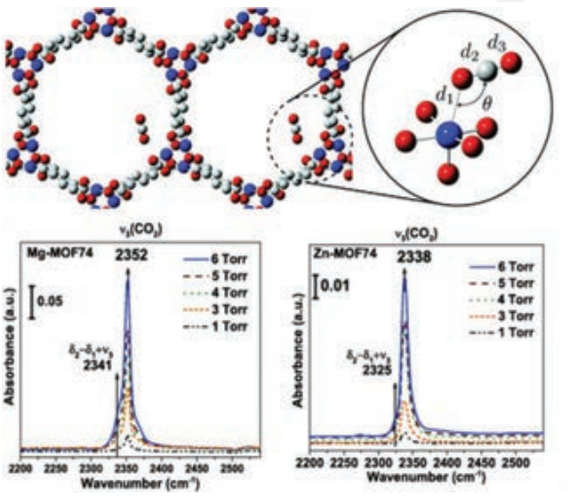

Figure 2. (Top) Illustration of CO_2 absorbed in Zn, Mg-MOF-74. (Bottom) IR absorption spectra of CO_2 absorbed into Mg-MOF-74 (bottom left) and Zn-MOF-74 (bottom right) at changing CO_2 pressure (1–6 Torr). Adapted with permission from [4]. Copyrighted by the American Physical Society.

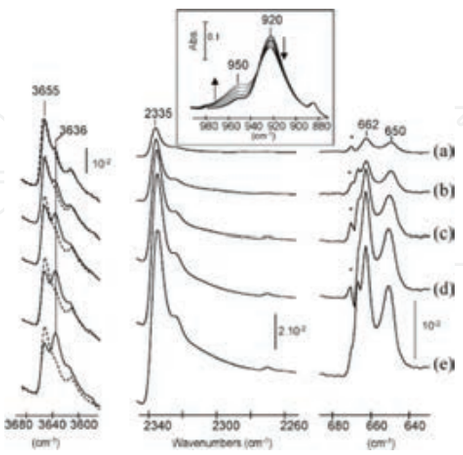

Figure 3. CO_2 introduction on MIL-53 (Cr) activated at 473 K. Spectra of activated MIL-53(Cr) deposited on silicon wafer (dotted lines) in three regions and then after introduction of increasing CO_2 equilibrium pressures into the cell (full lines): (a) 1066 Pa, (b) 2400 Pa, (c) 3850 Pa, (d) 5000 Pa, (e) 5850 Pa. Inset: perturbation of the δ(OH) mode upon CO_2 adsorption. Reproduced from [6] with permission of The Royal Society of Chemistry.

MOF $H_3[(Cu_4Cl)_3(BTTri)_8]$(H_3BTTri = 1,3,5-tri(1H- 1,2,3-triazol-4-yl)benzene) functionalized with N, N′-dimethylethylenediamine (mmen) shows significantly enhanced CO_2 adsorption with exceptional large isosteric heat of CO_2 around 96 kJ/mol [9]. The strong interaction of amine group of mmen with CO_2 molecules was directly proved by diffuse reflectance infrared Fourier-transform spectroscopy (DRIFTS) measurements. Upon dosing CO_2 to the sample with increasing pressure, the intensity of ν(N—H) band at 3283 cm^{-1} is significantly weakened and a new band at 1669 cm^{-1} appears, suggesting the formation of zwitterionic carbamates. N—H stretching band returns to back by regeneration of the solid under vacuum and heating to 60°C.

A very recent work shows that diamine-appended metal-organic frameworks M_2(dobpdc) ($dobpdc^{4-}$ = 4,4′-dioxidobiphenyl-3,3′-dicarboxylate), an expanded variant of the well-studied metal-organic framework MOF-74, with N,N′-dimethylethylenediamine (mmen) can behave as "phase change" adsorbents, with unusual step-shaped CO_2 adsorption isotherms that shift markedly with temperature [10]. In the unprecedented cooperative process it was found that, above a metal-dependent threshold pressure, CO_2 molecules insert into metal-amine bonds, inducing the reorganization of ammine into well-ordered chains of ammonium carbamate. **Figure 4** shows the insertion mechanism for CO_2 adsorption and spectral evolution upon cooling process. The formation of ammonium carbamate was confirmed by detecting the ν(C═O) mode at 1690 cm^{-1}, ν(C—N) at 1334 cm^{-1}, and broadening of ν(N—H) band, characteristic features of ammonium.

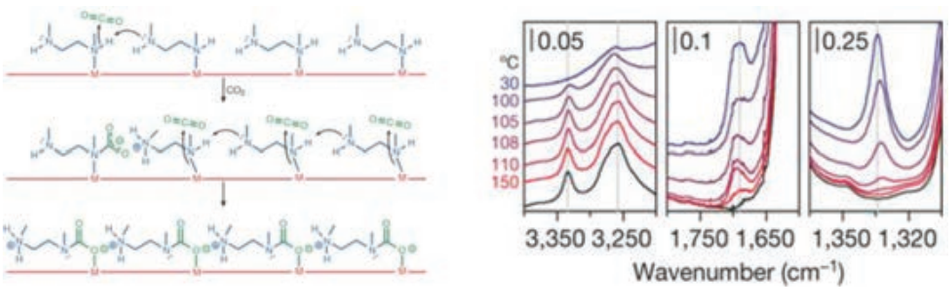

Figure 4. (Left) A cooperative insertion mechanism for CO_2 adsorption. (Right) Infrared spectra on dosing an activated sample of mmen-Mg_2(dobpdc) (black) with CO_2 and cooling from 150°C to 30°C (red to blue) under 5% CO_2 in N_2. The three different regions show bands corresponding to N—H (left), C—O (middle), and C—N (right) stretching vibrations. Reprinted by permission from Macmillan Publishers Ltd: [Nature] [10], copyright (2015).

CO_2 molecules are also stimuli to induce the structural transformation of some flexible MOFs. One of the earliest reports was CO_2 adsorption in chromium terephthalate MIL-53 [11]. CO_2 isotherm exhibits two-step adsorption and combined study of *in situ* diffraction and IR measurement provides clear explanation to this observation: after the first portion of CO_2 is absorbed into degassed solid, the host-guest interactions force the framework to close and cell to shrink. A further adsorption of CO_2 between 5 and 10 bar, reopens the framework while accepting additional CO_2 molecules into a newly formed channel. The strong interaction of CO_2 with the frameworks involves the formation of electron-donor-acceptor complexes between C atom of molecules and electron-donor center OH group of the framework, which was deduced from bending mode β(CO_2) splitting and ν(OH) mode red shift by *in situ* IR

http://dx.doi.org/10.5772/64906

spectroscopy. The pore opening phenomenon was also observed in CO_2 adsorption in $Zn_2(bpdc)_2(bpee)$ [12]. Raman and IR spectroscopy are combined together to investigate the CO_2 molecules interaction with $Zn_2(bpdc)_2(bpee)$ and found that interaction of CO_2 with the framework weakens the C—C inter-ring of the bpdc ligand, allowing it to rotate slightly around the monodentate connectivity C—O—Zn node. This rotation causes a series of changes resulting in pore opening, which is responsible for the preferential adsorption of CO_2 over N_2. Raman spectra in **Figure 5** shows the spectroscopic evidences for these changes: that the C—C inter-ring stretching in the bpdc ligand at 1296 cm^{-1} undergoes a red shift of ~–3 cm^{-1} and coordinated C—O symmetric stretching at 1355 cm^{-1} blue shift by ~+10 cm^{-1}, A ~+4 cm^{-1} blue shift of the band at 1644 cm^{-1} corresponding to the C═C stretching in the ethylene of the bpee ligand, is also observed. DFT calculations provide the support for the qualitative picture derived from the experimental analysis that more energetically favorable positions for the CO_2 molecules are closer to the C—C bond of the bpee and the C—C bond of the bpdc instead of their benzene and pyridine rings.

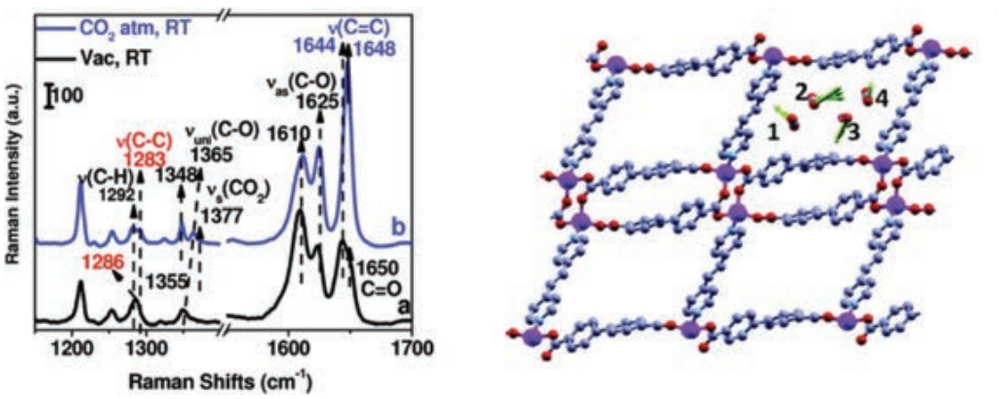

Figure 5. (Left) Raman spectra of activated $Zn_2(bpdc)_2(bpee)$ in a vacuum and after introduction of 1 atm of CO_2 at room temperature; (right) adsorption sites of CO_2 in complete occupation in $Zn_2(bpdc)_2(bpee)$ determined by vdW-DFT, where each pore within a unit cell is occupied by four CO_2 molecules. Reprinted with permission from [12]. Copyright (2011) American Chemical Society.

2.3. Reactive gas molecules

Water stability is a main concern for any potential applications of MOFs in industrial settings because moisture is ubiquitous in the environment, i.e., complete removal of H_2O from gas sources is difficult. Many widely investigated MOFs, particularly built by carboxylate acid ligand such as MOF-5 [13], MOF-177 [14], HKUST-1 [15], and MOF-74 [16] are susceptible to reaction with moisture. Understanding the degradation mechanism is a complex problem because there are a variety of independent factors that play a critical role in the stability of MOFs. However, the metal-ligand bond is regarded as the weakest point of a MOF structure. To decouple the effects of metal-ligand bond from other factors such as topology, porosity, and surface areas on the structural stability of MOFs, two types of prototypical and representative isostructure MOFs with different metal centers: (1) MOFs $M(bdc)(ted)_{0.5}$ [M = Cu^{2+}, Zn^{2+}, Ni^{2+}, Co^{2+}] with saturated metal centers and (2) MOF-74 [$M_2(dobdc)$, M = Mg^{2+}, Zn^{2+}, Ni^{2+}, Co^{2+}]

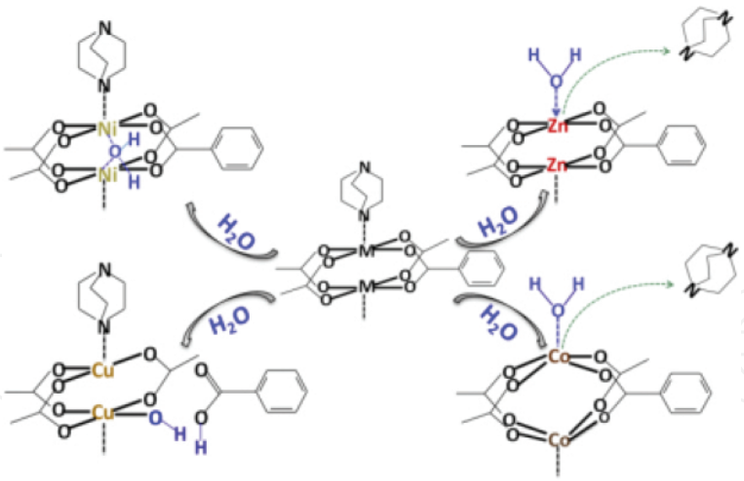

Figure 6. Schematic illustration of decomposition pathway of M(bdc)(ted)$_{0.5}$ [M = Cu, Zn, Ni, Co] reaction with D_2O molecules. Reprinted with permission from [17]. Copyright (2012) American Chemical Society.

with unsaturated metal centers were chosen for study [17, 18]. The former involves a secondary building unit (metal center configuration) that is very common to MOFs. The latter, referred to as MOF-74, is one of the most characterized materials for single gas adsorption as it is one of the best carbon capture materials. Combining spectroscopy methods (*in situ* infrared absorption and Raman) and powder X-ray diffraction, it was found that the stability of MOF in the presence of water vapor critically depends on their structure and the specific metal cation in the building units; and that water condensation inside pores, which is highly dependent on external vapor pressure and temperature, is the critical phenomenon that induces the hydrolysis reaction. In the case of M(bdc)(ted)$_{0.5}$, the metal-bdc bond is the most vulnerable for Cu(bdc)(ted)$_{0.5}$, while the metal-ted bond is first attacked for the Zn and Co analogs. In contrast, Ni(bdc)(ted)$_{0.5}$ remains stable under conditions where all other M(bdc)(ted)$_{0.5}$ materials are chemically attacked as shown in **Figure 6**. In the case of M_2(dobdc), or MOF-74, the weak link is the phenolate-metal bond. At room temperature, water is molecularly adsorbed inside the MOF channel. Above 150°C, the water molecule is dissociatively adsorbed at the metal-oxygen group with OH adsorption directly on the metal center and H adsorption on the bridging O of the phenolate group. Interestingly, the latter O—H bond is only detected when D_2O is used due to the strong vibrational coupling of the O—H bending vibration to the dobdc linker vibrations (see **Figure 7**). In contrast, the O—D bending vibration is fully decoupled from the linker vibrations (i.e., behaves as a local vibrational mode) leading to a strong, sharp, and detectable absorption band. Due to the passivation of open metal sites by hydroxyl group, the MOFs compounds lose a substantial fraction of their original gas uptake capacity.

NO adsorption has been studied before in Ni, Co-MOF-74 by isotherm, X-ray diffraction infrared and Raman spectroscopy, showing that NO interacts strongly with metal centers, forming NO coordination adduct with a binding energy of 90–92 kJ/mol [19, 20]. Infrared spectra shows that the stretching band ν(NO) of adsorbed NO molecules appears at a frequency between 1845 and 1838 cm^{-1} as coverage increases (see **Figure 8**). The red shift from the gas phase value at 1876 cm^{-1} indicates the interaction between NO and Ni-MOF-74 involves

http://dx.doi.org/10.5772/64906

back donation of d electrons from the metal to the antibonding orbital of nitrosyl group, therefore weakening N—O bond. The coverage dependent of ν(NO) stretching frequency suggest dipole-dipole interaction of adsorbed NO molecules. By gradually dosing the water vapor on the NO loaded sample, infrared spectra of **Figure 8** shows that NO is gradually removed. This ability of water displacing preadsorbed NO in slow kinetics make this materials a promising candidate for NO delivery in biological tissues.

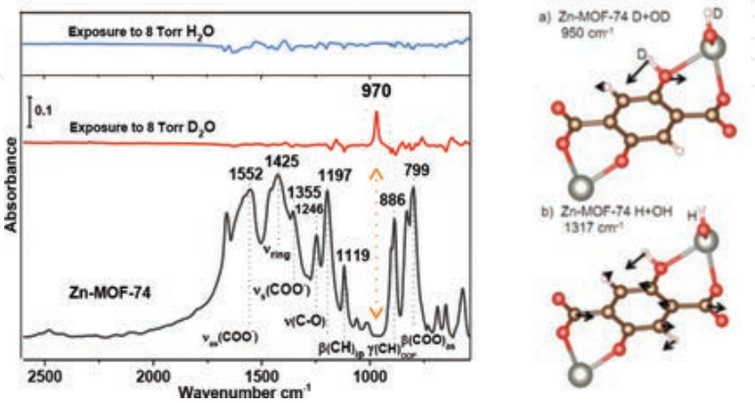

Figure 7. (Left) IR spectra of Zn-MOF-74 exposed to H_2O (blue) and D_2O (red), referenced to the activated MOF spectra, compared with IR absorption spectra of activated MOF-74, referenced to the KBr pellet; (right) calculated vibrational modes of (a) Zn-MOF-74 with dissociated D_2O (D + OD) at 950 cm^{-1}, (b) Zn-MOF-74 with dissociated H_2O (H + OH) at 1317 cm^{-1}. Reprinted with permission from [18]. Copyright (2014) American Chemical Society.

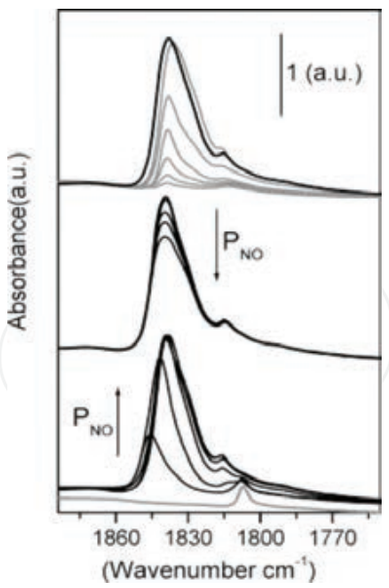

Figure 8. (Bottom) IR spectra of increasing NO equilibrium pressures dosed at RT on Ni-MOF-74 (equilibrium p_{max} = 0.1 mbar). Bold gray curve, vertically translated for clarity, reports the spectrum collected before NO dosage. (Middle) Spectra obtained upon successive progressive outgassing of loaded NO. (Top) Effect of water dosage on the irreversible NO (last spectrum of the middle part). Black spectra report the effect of 0.1 mbar NO dosage. Gray curves show the further interaction of water, at the vapor pressure as a function of contact times (up to 10 min). Reprinted with permission from [19]. Copyright (2008) American Chemical Society.

CO is demonstrated to be reversibly adsorbed in MOF-74 (M = Mg, Mn, Fe, Co, Ni, Zn) analogies with the binding strength following by the order of Ni > Co > Fe > Mg > Mn > Zn [21]. This sequence is in distinct contrast to that observed for CO_2 adsorption in these materials. The molecular adsorption configurations are shown in **Figure 9**. While CO_2 interaction with metal ions of MOF-74 frameworks is predominately electrostatic, CO coordination also involves σ and π orbital interactions, as being probed by infrared spectroscopy. For instance, CO exhibits a small blue shift in Fe, and Co-MOF-74 compared to Mg and Zn-MOF-74 since π back-donation in Fe and Co weaken the C-O bond, however, Mg^{2+} ions lack d electrons and unable to back-donate into the empty CO orbitals and Zn^{2+} ions has full occupied 3d orbital and are not available to accept σ charge donation from CO.

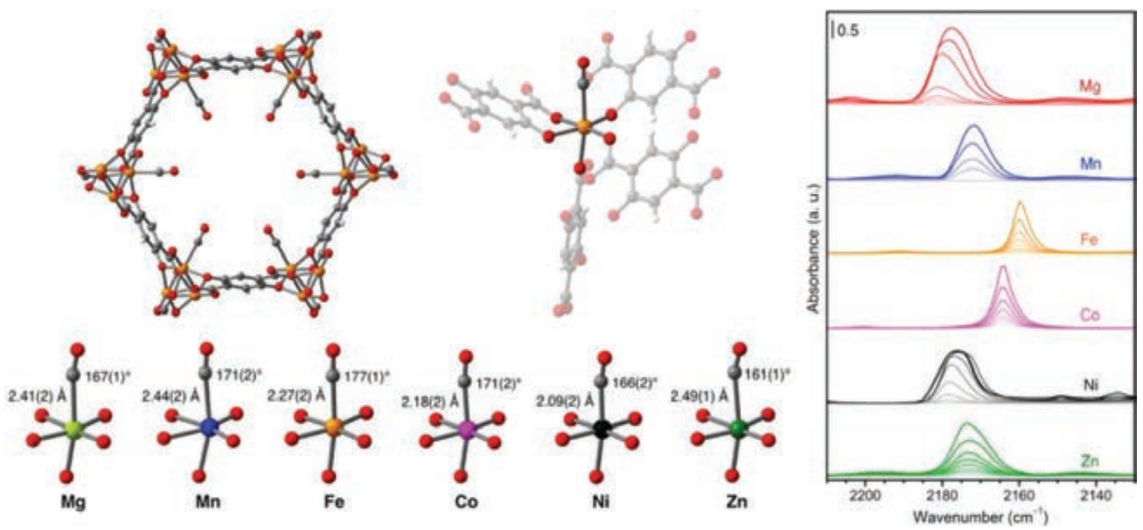

Figure 9. (Upper left) Structures from powder neutron diffraction. A view down a channel (along the *c* axis) in the structure of Fe_2(dobdc)·1.5CO, as determined by Rietveld analysis of powder neutron diffraction data and (upper right) coordination environment for a single Fe^{2+} site in Fe_2(dobdc)·1.5CO; (bottom) first coordination sphere for the M^{2+} ions in M_2(dobdc)·1.5CO, with M—CO distances and M—C—O angles indicated; (Right) Background subtracted FTIR spectra of M_2(dobdc) collected at 77 K in the presence of CO. Light to dark lines represent increasing CO coverage on samples. Reprinted with permission from [21]. Copyright (2014) American Chemical Society.

O_2 is IR inactive and nonreactive to many MOFs materials, however, gas adsorption isotherms at 298 K indicate that Fe_2(dobdc) binds O_2 preferentially over N_2 via electron transfer interaction, with an irreversible capacity of 9.3 wt%, corresponding to the adsorption of one O_2 molecule per two iron centers [22]. Infrared spectra show that upon oxygenation at low temperature. A partially reduced (near superoxo) O_2 species coordinated to FeII/III sites was observed at 1129 cm^{-1}, assigned to ν(O—O). The formation of iron(III)-peroxide species at 790 cm^{-1} was detected at room temperature. The charge-transfer interaction was also found in adsorption of O_2 in a Zn-MOF containing 7, 7, 8, 8-tetracyano-p-quinodimethane (TCNQ) ligand where organic linker is the active adsorption site. The large red shift of the sharp ν(O═O) band by 100 cm^{-1} was observed in IR spectra upon loading O_2 at 90 K [23]. This frequency shift is too large to be induced by the confinement effect alone. It suggests that O_2 molecules accommodated in TCNQ MOF have a partial negative charge, donated by electron rich organic linker.

http://dx.doi.org/10.5772/64906

SO_2 adsorption has been studied in MOFs materials such as IR-MOFs (which have the same underlying topology as MOF-5 [24], $M(bdc)(ted)_{0.5}$ [25], FMOF-2 [26], and NOTT-300 [27]). Among all studied structures, the uptake of SO_2 in $M(bdc)(ted)_{0.5}$ at room temperature is highest, 9.97 mol/kg at 1.13 bar [25]. The adsorption mechanism of SO_2 within this class of MOFs is further explored by *in situ* IR spectroscopy, finding that the major adsorbed SO_2 molecules contributing to the isotherm measurements are characterized by stretching bands at 1326 and 1144 cm^{-1}, −36 and −7 cm^{-1} (see **Figure 10**), red shift respectively from the unperturbed values of 1362 and 1151 cm^{-1} of gas phase. In addition, the IR spectra reveal the presence of another minor species at 1242 and 1105 cm^{-1} that is more strongly bound, requiring a higher temperature (~150°C) to remove. SO_2 adsorption also induces significant changes to the frameworks vibrational modes (see **Figure 10**): (1) a blue shift of the $\nu_{as}(COO)$ mode ($\Delta\nu$ = +56 cm^{-1}) and of the $\nu_s(COO)$ mode ($\Delta\nu$ = +39 cm^{-1}), and (2) a decrease in intensity of $\nu_{as}(CH_2)$, $\nu_s(CH_2)$, and $\nu(CH)$ modes at 2874, 2938, and 3076 cm^{-1}, respectively. Furthermore, the CH_2 rocking mode and benzene ring deformation mode σ_{12} are red shifted by −8 and −12 cm^{-1}. Calculations based on vdW-DF codes suggest that two adsorption configurations are possible for these SO_2 molecules. One geometry involves an SO_2 molecule bonded through its sulfur atom to the oxygen atom of the paddlewheel building unit and its two oxygen atoms to the C—H groups of the organic linkers by formation of hydrogen bonds. Such a configuration results in a distortion of the benzene rings, which is consistent with the experimentally observed shift of the ring deformation mode.

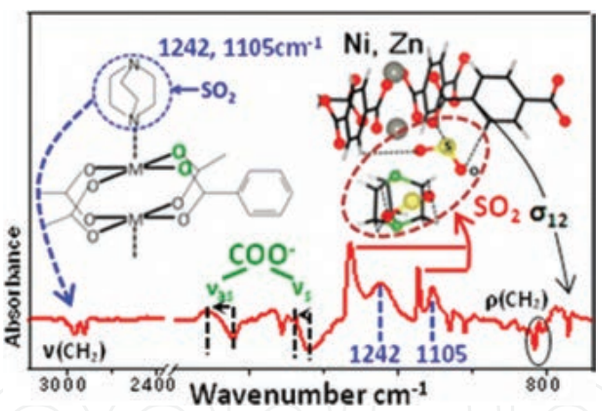

Figure 10. Snapshot of initial adsorption configuration models of SO_2 in $Zn(bdc)(ted)_{0.5}$ and IR absorption spectra after loading SO_2 at 256 Torr, recorded immediately after evacuation of gas phase (within 16 s). Reprinted with permission from [25]. Copyright (2013) American Chemical Society.

MOFs such as MIL-47 (V), MIL-53(Al, Cr) with saturated metal center show weak interaction with H_2S and adsorption/desorption behavior is completely reversible in isotherm measurement. For some MOFs structures MIL-101(Cr), HKUST-1 with unsaturated metal sites [28, 29], the adsorption of H_2S is quite reactive, leading to release of BTC ligand from coordination with copper metal center and the formation of carboxlyate C═O group as indicated by the appearing of a band at 1710 cm^{-1}. MOF-74 with nickel center shows a strong binding strength toward H_2S with an adsorption heat ΔH_{ads} of ~57 kJ/mol [30]. The PXRD pattern shows that the structure itself is stable under H_2S exposure, which is consistent with the observation from

IR spectra that most MOFs phonon modes are slightly affected. The molecular state of H_2S in Ni-MOF-74 is characterized by its clear IR features at 2626, 2614, and 1182 cm^{-1}, corresponding to asymmetric, symmetric stretching, and bending mode.

2.4. Coadsorption

Compared to the extensive studies that focus on the single component adsorption, the coadsorption of muticomponents remains scarcely investigated due in part to experimental difficulties, for instance, the isotherm of muticomponent adsorption, the composition of each species adsorbed can only be derived indirectly by measuring variation of gas-phase composition. Methods, such as mass spectrometry, have to be incorporated with isotherm measurements. *In situ* IR spectroscopy in conjunction with *ab initio* modeling can provide information on local bonding sites and exchange mechanisms, as demonstrated by recent work in prototypical structure MOF-74 [31]. Using CO_2 as a probe molecule, competitive coadsorption of CO_2 with a variety of small molecules (H_2O, NH_3, SO_2, NO, NO_2, N_2, O_2, and CH_4) in M-MOF-74 (M = Mg, Co, Ni) was investigated by infrared spectroscopy. Surprisingly, the displacement of CO_2 adsorbed at the metal center by other molecules such as H_2O, NH_3, SO_2, NO, NO_2, N_2, O_2, and CH_4 is mainly observed for H_2O and NH_3, even though SO_2, NO, and NO_2 have higher binding energies (~70–90 kJ/mol) to metal sites (Mg^{2+}, Ni^{2+}, Co^{2+}) than that of CO_2 (~38–48 kJ/mol) and slightly higher than that of water (~60–80 kJ/mol) as shown in **Figure 11**. The exchange process is differentiated by plotting the intensity of H_2O band ν(OH) ~above 2600 cm^{-1} and CO_2 band ν_{as} at 2341 cm^{-1} (see **Figure 12**). The uptake of water is dominated by transport; therefore, taking its complement (red curve in **Figure 12**) for the CO_2 release (gray curve) simulates what is expected if exchange kinetics

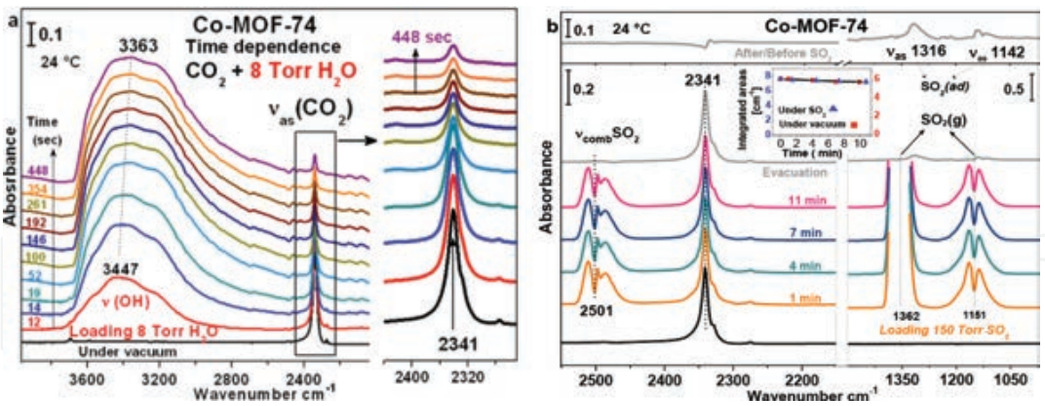

Figure 11. (Left, a) IR absorption spectra of 8 Torr H_2O (broad peak above ~2600 cm^{-1}) adsorbed into Co-MOF-74 with preloaded CO_2 (peak at 2341 cm^{-1}) as a function of time. All referenced to the activated MOF under vacuum (<20 mTorr). The black line in the bottom shows the absorption spectra of CO_2 before loading water. (Right, b) IR absorption spectra of activated and CO_2-preloaded Co-MOF-74 exposed to ~150 Torr SO_2. The bottom spectrum shows the adsorbed CO_2 in Co-MOF-74 under vacuum (<20 mTorr). The middle part shows the time-dependent spectrum during SO_2 exposure and the spectrum after evacuation of gas phase SO_2. The differential spectrum on the top right of (b) shows the spectrum recorded after loading SO_2 for 10 min and evacuation of gas phase, referenced to the spectrum before loading SO_2 as shown in the bottom black spectrum. Reprinted with permission from [31]. Copyright (2015) American Chemical Society.

were much faster than diffusion. It represents the amount of CO_2 displaced by water as it arrives at the CO_2 site. This simulated CO_2 concentration was specifically plotted to highlight that the measured CO_2 concentration (black curve in **Figure 12**) evolved more slowly (additional time is required for exchange since the barrier is not negligible). This simulated curve (based on the water intake) is then used to normalize the CO_2 absorption measurements, i.e., remove the transport part of the time evolution by subtracting the time due to transport (diffusion of water molecules to inner pores). The net result is shown in the inset of **Figure 12** that now represents only the exchange kinetics.

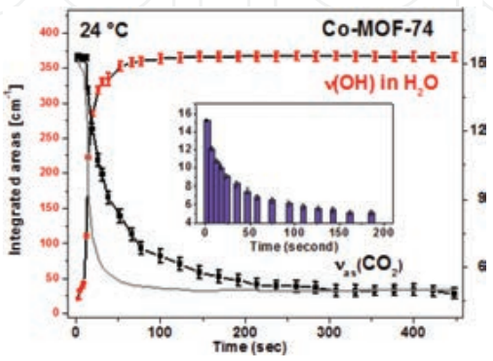

Figure 12. Evolution of integrated areas of the IR bands of water ν(OH) (red) and CO_2 $\nu_{as}(CO_2)$ (black) in Co-MOF-74 at 24°C. The inset purple bar curve shows the $\nu_{as}(CO_2)$ band evolution corrected by removing the water transport time (taken from the gray curve) and hence provides the intensity evolution solely controlled by exchange kinetics. Reprinted with permission from [31]. Copyright (2015) American Chemical Society.

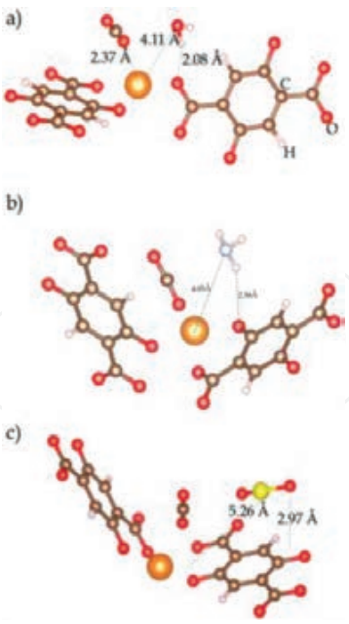

Figure 13. Adsorption configuration of the H_2O (top), NH_3 (middle), SO_2 (bottom) molecule on Mg-MOF-74 fully loaded with CO_2 molecules at the metal centers. Red, brown, gray, blue, and orange spheres denote O, C H, N, and Mg atoms, respectively. Parts of the MOF have been removed for visualization purposes. Reprinted with permission from [31]. Copyright (2015) American Chemical Society.

Ab initio simulations was performed to calculate the exchange barrier (activation energy) and study the reaction pathway for the $H_2O \rightarrow CO_2$ and $SO_2 \rightarrow CO_2$ exchange processes at the primate adsorption site of the open metal center. It was found that hydrogen bonding of H_2O or NH_3 molecules with the nearby oxygen of the organic linker facilitates the positioning of the H_2O oxygen atom toward the metal center and displacing the preadsorbed CO_2 molecule as shown in **Figure 13**. However, SO_2 (and other molecules without H atoms) are not able to do so and remain bound at a distant site of carbon ring from metal center. In order to displace the CO_2 molecules at metal site, SO_2 needs to break away from the attractive force of the initial adsorption sites to move to the meter center and overcomes a high energy barrier (~20 kJ/mol) than water molecules (~13 kJ/mol) to remove the preoccupied CO_2 molecules.

This important scientific finding revolutionized the understanding of MOF coadsorption by establishing that the displacement of one molecule by another within porous materials is a complex process that the energetics consideration alone cannot successfully predict. In other words, the binding energy at the most favorable adsorption site is not a sufficient indicator of the molecular stability in MOFs and kinetics of exchange process must be considered.

3. Conclusion

Vibrational spectroscopy has been proved to be the very informative technique to investigate the interaction of small gas molecules with metal organic frameworks. By examining subtle changes in the spectra of both adsorbate and adsorbent, insightful details regarding the adsorption mechanism are revealed. With the help of theoretical calculation, which provides direct access to many properties of the system, the experimental models are validated and a complete understanding of the adsorption behaviors can be derived.

For H_2, although free molecule is IR inactive, the stretching mode is activated and becomes observable once the molecule is polarized by binding to the surface. A wealth of information for the interaction details, i.e., binding site and geometry, interaction potential can be extracted by analyzing the peak position, intensity, and width.

For CO_2 molecules, both the perturbation of stretching and bending mode convey important information for the nature of interaction. For physical adsorption with lower binding energy (<50–60 kJ/mol), the stretching mode suffers a small shift (<15 cm^{-1}) compare to gas phase value and the bending mode is spitted due to the loss of degeneracy. If the molecules are chemically adsorbed with a high adsorption heat over 60–70 kJ/mol, IR adsorption features of new species such as carbamate can be observed. The structural modifications for functional groups are reflected by tracking the spectroscopic signatures.

For the reactive molecules such as H_2O, O_2, H_2S, SO, and NO adsorbing into MOFs, the crystalline structure is strongly modified and even become degraded. By examining the difference spectra before and after adsorption, the weak point of the complicated MOFs structure can be identified and reaction pathway can be also unveiled, which is crucial to design robust structure.

Finally, infrared spectroscopy provides an unique advantage to study the adsorption behaviors of mixture components since the vibrational modes of different molecules usually can be well distinguished in the infrared spectra. The occupation of actual adsorption sites for mixtures can be measured as a function of parameters such as time, temperature, and partial pressure. Recent works in measuring CO_2 competition with a variety of molecules, e.g., H_2O, NH_3, SO_2, NO, and NO_2 in MOF-74 show kinetics for exchange process is an important parameter which needs to be taken into account for coadsorption and separation process. It also underscores the need of combined studies, using spectroscopic methods and *ab initio* simulations to uncover the atomistic interactions of small molecules in MOFs that directly influence coadsorption.

Author details

Kui Tan* and Yves Jean Chabal

*Address all correspondence to: kuitannk@gmail.com

Department of Materials Science and Engineering, The University of Texas at Dallas, Richardson, Texas, USA

References

[1] Nijem N, Veyan JF, Kong L, Li K, Pramanik S, Zhao Y, Li J, Langreth DC, Chabal YJ. Interaction of molecular hydrogen with microporous metal organic framework materials at room temperature. J Am Chem Soc. 2010; 132(5): 1654–1664. DOI: 10.1021/ja908817n

[2] Nijem N, Veyan JF, Kong L, Wu H, Zhao Y, Li J, Langreth DC, Chabal YJ. Molecular hydrogen "Pairing" interaction in a metal organic framework system with unsaturated metal centers (MOF-74). J Am Chem Soc. 2010; 132(42): 14834–14848. DOI:10.1021/ja104923f

[3] Garrone E, Otero Arean C. Variable temperature infrared spectroscopy: a convenient tool for studying the thermodynamics of weak solid-gas interactions. Chem Soc Rev. 2005; 34(10): 846–857. DOI:10.1039/b407049f

[4] Yao Y, Nijem N, Li J, Chabal YJ, Langreth DC, Thonhauser T. Analyzing the frequency shift of physiadsorbed CO_2 in metal organic framework materials. Phys Rev B. 2012; 85(6): 064302. DOI:10.1103/PhysRevB.85.064302

[5] FitzGerald SA, Schloss JM, Pierce CJ, Thompson B, Rowsell JLC, Yu K, Schmidt JR. Insights into the anomalous vibrational frequency shifts of CO_2 adsorbed to metal sites

in microporous frameworks. J Phys Chem C. 2015; 119(10): 5293–5300. DOI:10.1021/jp5104356

[6] Vimont A, Travert A, Bazin P, Lavalley JC, Daturi M, Serre C, Ferey G, Bourrelly S, Llewellyn PL. Evidence of CO_2 molecule acting as an electron acceptor on a nanoporous metal-organic-framework MIL-53 or $Cr^{3+}(OH)(O_2C—C_6H_4—CO_2)$. Chem Commun. 2007; (31): 3291–3293. DOI:10.1039/b703468g

[7] Kazarian SG, Vincent MF, Bright FV, Liotta CL, Eckert CA. Specific intermolecular interaction of carbon dioxide with polymers. J Am Chem Soc. 1996; 118(7): 1729–1736. DOI:10.1021/ja950416q

[8] Gascon J, Aktay U, Hernandez-Alonso MD, van Klink GPM, Kapteijn F. Amino-based metal-organic frameworks as stable, highly active basic catalysts. J Catal. 2009; 261(1): 75–87. DOI: j.jcat.2008.11.010

[9] McDonald TM, D'Alessandro DM, Krishna R, Long JR. Enhanced carbon dioxide capture upon incorporation of N,N[prime or minute]-dimethylethylenediamine in the metal-organic framework CuBTTri. Chem Sci. 2011; 2(10): 2022–2028. DOI:10.1039/c1sc00354b

[10] McDonald TM, Mason JA, Kong X, Bloch ED, Gygi D, Dani A, Crocella V, Giordanino F, Odoh SO, Drisdell WS, Vlaisavljevich B, Dzubak AL, Poloni R, Schnell SK, Planas N, Lee K, Pascal T, Wan LF, Prendergast D, Neaton JB, Smit B, Kortright JB, Gagliardi L, Bordiga S, Reimer JA, Long JR. Cooperative insertion of CO_2 in diamine-appended metal-organic frameworks. Nature. 2015, advance online publication. DOI: 10.1038/nature14327

[11] Serre C, Bourrelly S, Vimont A, Ramsahye NA, Maurin G, Llewellyn PL, Daturi M, Filinchuk Y, Leynaud O, Barnes P, Férey G. An explanation for the very large breathing effect of a metal–organic framework during CO_2 adsorption. Adv Mater. 2007; 19(17): 2246–2251. DOI: 10.1002/adma.200602645

[12] Nijem N, Thissen P, Yao Y, Longo RC, Roodenko K, Wu H, Zhao Y, Cho K, Li J, Langreth DC, Chabal YJ. Understanding the preferential adsorption of CO_2 over N_2 in a flexible metal–organic framework. J Am Chem Soc. 2011; 133(32): 12849–12857. DOI: 10.1021/ja2051149

[13] Huang L, Wang H, Chen J, Wang Z, Sun J, Zhao D, Yan Y. Synthesis, morphology control and properties of porous metal–organic coordination polymers. Microporous Mesoporous Mater. 2003; 58(2): 105–114. DOI: 10.1016/S1387-1811(02)00609-1

[14] Li Y, Yang RT. Gas adsorption and storage in metal-organic framework MOF-177. Langmuir. 2007; 23(26): 12937–12944. DOI: 10.1021/la702466d

[15] DeCoste JB, Peterson GW, Schindler BJ, Killops KL, Browe MA, Mahle JJ. The effect of water adsorption on the structure of the carboxylate containing metal-organic frame-

works Cu-BTC, Mg-MOF-74 and UiO-66. J Mater Chem. 2013; 1(38): 11922–11932. DOI: 10.1039/c3ta12497e

[16] Kizzie AC, Wong-Foy AG, Matzger AJ. Effect of humidity on the performance of microporous coordination polymers as adsorbents for CO_2 capture. Langmuir. 2011; 27(10): 6368–6373. DOI: 10.1021/la200547k

[17] Tan K, Nijem N, Canepa P, Gong Q, Li J, Thonhauser T, Chabal YJ. Stability and hydrolyzation of metal organic frameworks with paddle-wheel SBUs upon hydration. Chem Mater. 2012; 24(16): 3153–3167. DOI:10.1021/cm301427w

[18] Tan K, Zuluaga S, Gong Q, Canepa P, Wang H, Li J, Thonhauser T, Chabal YJ. Water reaction mechanism in metal organic frameworks with coordinatively unsaturated metal ions: MOF-74. Chem Mater. 2014; 26(23): 6886–6895. DOI:10.1021/cm5038183

[19] Bonino F, Chavan S, Vitillo JG, Groppo E, Agostini G, Lamberti C, Zecchina A, Solari PL, Kongshaug KO, Bordiga S. Local structure of CPO-27-Ni metallorganic framework upon dehydration and coordination of NO. Chem Mater. 2008; 20(15): 4957–4968. DOI: 10.1021/cm052191g

[20] McKinlay AC, Xiao B, Wragg DS, Wheatley PS, Megson IL, Morris RE. Exceptional behavior over the whole adsorption–storage–delivery cycle for NO in porous metal organic frameworks. J Am Chem Soc. 2008; 130(31): 10440–10444. DOI:10.1021/ja801997r

[21] Bloch ED, Hudson MR, Mason JA, Chavan S, Crocellà V, Howe JD, Lee L, Dzubak AL, Queen WL, Zadrozny JM, Geier SJ, Lin LC, Gagliardi L, Smit B, Neaton JB, Bordiga S, Brown CM, Long JR. Reversible CO binding enables tunable CO/H_2 and CO/N_2 separations in metal-organic frameworks with exposed divalent metal cations. J Am Chem Soc. 2014; 136(30): 10752–10761. DOI:10.1021/ja505318p

[22] Bloch ED, Murray LJ, Queen WL, Chavan S, Maximoff SN, Bigi JP, Krishna R, Peterson VK, Grandjean F, Long GJ, Smit B, Bordiga S, Brown CM, Long JR. Selective binding of O_2 over N_2 in a redox-active metal-organic framework with open iron(II) coordination sites. J Am Chem Soc. 2011; 133(37): 14814–14822. DOI: 10.1021/ja205976v

[23] Shimomura S, Higuchi M, Matsuda R, Yoneda K, Hijikata Y, Kubota Y, Mita Y, Kim J, Takata M, Kitagawa S. Selective sorption of oxygen and nitric oxide by an electron-donating flexible porous coordination polymer. Nat Chem. 2010; 2(8): 633–637. DOI: 10.1038/nchem.684

[24] Britt D, Tranchemontagne D, Yaghi OM. Metal-organic frameworks with high capacity and selectivity for harmful gases. Proc Natl Acad Sci. 2008; 105(33): 11623–11627. DOI: 10.1073/pnas.0804900105

[25] Tan K, Canepa P, Gong Q, Liu J, Johnson DH, Dyevoich A, Li J, Thonhauser T, Chabal YJ. Mechanism of preferential adsorption of SO_2 into two microporous paddle wheel

frameworks M(bdc)(ted)$_{0.5}$. Chem Mater. 2013; 25(23): 4653–4662. DOI:10.1021/cm401270b

[26] Fernandez CA, Thallapally PK, Motkuri RK, Nune SK, Sumrak JC, Tian J, J. Liu. Gas-induced expansion and contraction of a fluorinated metal–organic framework. Cryst Growth Des. 2010; 10(3): 1037–1039. DOI: 10.1021/cg9014948

[27] Yang S, Sun J, Ramirez-Cuesta AJ, Callear SK, DavidWilliam IF, Anderson DP, Newby R, Blake AJ, Parker JE, Tang CC, Schröder M. Selectivity and direct visualization of carbon dioxide and sulfur dioxide in a decorated porous host. Nat Chem. 2012; 4(11): 887–894. DOI:10.1038/nchem.1457

[28] Hamon L, Serre C, Devic T, Loiseau T, Millange F, Férey G, Weireld GD. Comparative study of hydrogen sulfide adsorption in the MIL-53(Al, Cr, Fe), MIL-47(V), MIL-100(Cr) and MIL-101(Cr) Metal–organic frameworks at room temperature. J Am Chem Soc. 2009; 131(25): 8775–8777. DOI: 10.1021/ja901587t

[29] Petit C, Mendoza B, Bandosz TJ. Hydrogen sulfide adsorption on MOFs and MOF/graphite oxide composites. Chem Phys Chem. 2010; 11(17) 3678–3684. DOI: 10.1002/cphc.201000689

[30] Chavan S, Bonino F, Valenzano L, Civalleri B, Lamberti C, Acerbi N, Cavka JH, Leistner M, Bordiga S. Fundamental aspects of H_2S adsorption on CPO-27-Ni. J Phys Chem C. 2013; 117(30): 15615–15622. DOI: 10.1021/jp402440u

[31] Tan K, Zuluaga S, Gong Q, Gao Y, Nijem N, Li J, Thonhauser T, Chabal YJ. Competitive coadsorption of CO_2 with H_2O, NH_3, SO_2, NO, NO_2, N_2, O_2 and CH_4 in M-MOF-74 (M = Mg, Co, Ni): The role of hydrogen bonding. Chem Mater. 2015; 27(6): 2203–2217. DOI: 10.1021/acs.chemmater.5b00315